J Sol-Gel Sci Technol (2007) 43:251–258
DOI 10.1007/s10971-007-1576-0

ORIGINAL PAPER

Synthesis and characterization of sol–gel derived glass-ceramic and its corrosion protection on 316L SS

U. Vijayalakshmi · S. Rajeswari

Received: 7 December 2006 / Accepted: 4 April 2007 / Published online: 8 May 2007

Abstract Glass-ceramic was prepared by sol–gel method using $Ca(NO_3)_2{\cdot}4H_2O$ and P_2O_5 as Ca and P precursors, respectively. In order to improve the bioactivity of the implant material, glass-ceramic (β-$Ca_2P_2O_7$) coating was developed on 316L SS substrate by spin coating method. Coating was annealed at different temperatures and its corrosion resistance was evaluated by electrochemical polarization and impedance analysis using Ringer's solution as electrolyte. The results from the present study, show excellent corrosion resistance for coated 316L SS, corroborated by the high values of charge transfer resistance from impedance analysis and higher breakdown and repassivation potential with the corresponding lower current density from polarization measurements. Based on the results, the glass-ceramic coating on 316L SS can be considered as a corrosion resistant material.

Keywords Sol–gel · Glass-ceramic · Corrosion · Impedance

1 Introduction

Metals and alloys are used in restoration of anatomical structures for centuries owing to their superior mechanical properties. However, the degradation of most metals implanted in the human body has narrowed the choice of clinically usable metals and alloys to mainly stainless steels, cobalt-chromium, and titanium alloys [1]. These metallic devices are unique that they are exposed to living cells, tissues, and biological fluids, which are not only dynamic but are also a hostile environment for the survival of the implant. Titanium alloys are employed for orthopedic implants due to their excellent combination of biocompatibility, corrosion resistance, and mechanical properties. However, toxicity of alloying elements and a high elastic modulus compared to bone has been reported as disadvantages. Although titanium has excellent corrosion resistance, if any of the alloying elements are released into the tissue by corrosion or wear, various tissue reactions can occur ranging from a mild response such as discoloration of surrounding tissue, to a severe one causing pain and even loosening of the implant. Discoloration of surrounding tissues due to debris particles is the main drawback [2]. Type 316L stainless steel (SS) is widely used for implantation purposes in orthopeadics owing to their corrosion resistance, mechanical properties, and low cost. However, clinical results have shown that they are susceptible to localized corrosion attack in the human body environment. Several incidences of failures of such devices have demanded the application of biocompatible and corrosion resistant coatings and surface modification of the alloys.

Thus, surface modification of implantable materials can be a powerful tool for improving their biocompatibility. The most common techniques used in surface modification are by coating with HAP, glass-ceramic, glass, and by polymeric coating. Different calcium phosphate materials exhibit different resorption properties and it depends on Ca/P ratio, degree of crystallinity and crystal structure. Specifically, various coatings by sol–gel processing have been studied for corrosion protection of SS [3–6]. However, some glass-ceramic coatings have shown higher bioactivity and the bioactivity of implant alloys is primarily related to their corrosion behavior [7]. Promising results have been obtained by sol–gel coatings, which act as a barrier against oxidation and corrosion of stainless steel

U. Vijayalakshmi (✉) · S. Rajeswari
Department of Analytical chemistry, University of Madras, Guindy Campus, Chennai 600 025, India
e-mail: lakesminat@yahoo.com

[8, 9]. Thus, sol–gel coatings could be an alternative way for improving the performance of metallic prosthesis. Chin et al. reported the development of resorbable pyro phosphate glass from CaO and P_2O_5 precursors and its use for tooth and bone implant applications [10]. Also, the preparation of pyro phosphate glass-ceramic has received more attention in the biomedical field.

In the present study, a highly resorbable glass-ceramic was prepared. The formation of pyro phosphate glass-ceramic with no other secondary phases was confirmed by fourier transform infra red spectroscopy (FT-IR) and XRD analysis. In order to design and produce a desired coating for implantation purposes, the corrosion resistance behavior of the glass-ceramic coated 316L SS was evaluated by electrochemical studies.

2 Experimental

2.1 Preparation of glass-ceramic

Anhydrous ethanol was freshly distilled and was used as a solvent. All the experiments were carried out in a dry atmosphere with vacuum manifolds for air sensitive reagents. An ethanol solution of $Ca(NO_3)_2{\cdot}4H_2O$ and a non-alkoxide based P_2O_5 was selected as calcium and phosphorus precursors respectively. The hydrolysis activity of P_2O_5 was induced by refluxing in a water bath at 90 °C for 24 h. The refluxed P_2O_5 solution has phosphorous species mainly in the form of $PO(OH)(OR)_2$ and $PO(OH)_2(OR)$ with a small amount of H_3PO_4 [11, 12]. Since these oxy alkoxide phosphorous species have good reactivity with the calcium precursor, it was slowly added to the solution containing 1 M calcium nitrate tetrahydrate to obtain a Ca/P ratio of 1.00. Then, the mixed solution was aged in an oil bath at 90 °C for 16 h.

In order to understand the formation process of calcium pyrophosphate, the obtained gel was transformed into powders by transferring it into a petri dish and heated at 150 °C for 16 h. Finally, the as prepared powder was sintered at 900 °C.

2.2 Characterization of the powder sample

2.2.1 Chemical analysis

The sintered powder sample was chemically analyzed for the determination of Calcium and Phosphorous. Calcium was determined by complexometric titration using EDTA. Phosphorous was determined by gravimetric method using magnesia mixture and ammonium citrate. An average of four determinations was taken. The Calcium and Phosphorous ratio was found to be 1.00, which could be due to the formation of pyrophosphate ions.

The as dried and sintered powder was characterized by FT-IR in the range of 400–4000 cm^{-1} using a SHIMADZU model 8300 spectrophotometer using KBr pellet technique (0.1 wt%) and by X-ray diffraction technique (XRD) for phase identification. The XRD patterns were recorded in an x-ray diffractometer (Seifert Jso-Debyerex-2002) with a step size of 0.02° and a scan rate of 1 °C/min with CuKα radiation (λ = 1.54056 Å).

2.3 Characterization of the coatings

2.3.1 Sample preparation

Polished surface of the metal plays an important role in the electrochemical evaluation of the sol–gel coating. The 316L SS samples were polished using silicon carbide grit sheets of 220, 320, 400, 600, 800, and 1,000 grit. The polished specimens were degreased with acetone and finally washed with distilled water. The elemental composition of 316L SS alloy is given in Table 1.

2.3.2 Sol–gel spin coatings

The sol was spun on the polished 316L SS substrates by spin coating method at a constant speed of 2,000 RPM/Min at room temperature. The single layer-coated substrates were immediately transferred into an oven at 150 °C and held for 10 min. In order to increase the thickness of the coating, the above process was repeated for three times and finally it was sintered at various temperatures (300, 800, and 900 °C). All the coated substrates after sintering treatments were regularly observed under the optical microscope (NISSHO Optical (N.S.K), Japan), to determine the defects/damages that could occur during this process and the deposited films were characterized through electrochemical study.

The instrument Philips 501 Scanning Electron Microscope (SEM) equipped with Energy Dispersive X- ray microanalysis (EDAX) was used for the determination of micro structural and elemental analysis of the coating sintered at 800 °C.

Table 1 Elemental composition of 316L SS

Element	Cr	Ni	Mo	Mn	P	C	S	Si	Fe
Composition (Wt%)	18.00	12.00	2.50	1.70	0.04	0.02	0.01	0.15	Balance

Adhesive strength of the coating layer was tested using a testing machine Shimadzu Universal Testing machine, AG-25TA) with the cross head speed of 2 mm/min. Two metallic cylinders with 8 mm in diameter were attached to both sides of the samples, of which one side of the sample was mounted on the epoxy glue. The glue was cured at a temperature of 175 °C for 60 min and the other side was coated with HAP. For each sample five measurements were tested.

2.3.3 Cyclic polarization study

Ringer's solution that simulates body fluid conditions was used as electrolyte in the evaluation of electrochemical behavior of the sol–gel coated 316L SS. The chemical composition of the solution is given in Table 2. The electrochemical cell of 500 mL capacity fitted with Saturated Calomel Electrode (SCE) was used as a reference electrode. Platinum foil and 316L SS were used as auxiliary and working electrode respectively. The working electrode having test surface of 1 cm^2 was used for all the experiments. The cyclic polarization study was carried out by increasing the potential in a noble direction at a scan rate of 1 mV/s until the pitting potential was observed. The potential at which there was a smooth increase in the current density is termed as pitting potential or breakdown potential (E_b). The sweep direction was reversed after reaching an anodic current density of 3 mA/cm^2. The potential at which reverse scan meets the passive region is termed as the repassivation potential (E_p). Cyclic polarization studies were carried out using vibrant potentiostat/galvanostat model No: VSM/CS/30, where the electrochemical interface was controlled by software.

2.3.4 Electrochemical impedance study

EIS measurements were carried out using (Gill AC Potentiostat/Galvanostat frequency response analyser, UK). The measurements of the EIS were performed at OCP using a frequency scan from 10,000 Hz to 0.1 Hz. Both Nyquist and Bode plot was analyzed by software analyzer to determine the parameters such as charge transfer resistance (R_{ct}) and the double layer capacitance (C_{dl}). The coatings on 316L SS were immersed in the test electrolyte (Ringer's solution) for 60 min in order to establish a steady state between the electrolyte and the coating. The change in potential with respect to time was monitored until the potential reaches a steady state. The potential of the working electrode with respect to reference electrode after stabilization period is termed as open circuit potential (OCP).

Table 2 Chemical composition of Ringer's solution

S. No	Reagent	Wt (g/L)
1	NaCl	8.60
2	KCl	0.60
3	$CaCl_2{\cdot}2H_2O$	0.66

3 Results and discussion

In the sol–gel process, the calcium and phosphorous precursors are converted to amorphous gels through hydrolysis and condensation reactions, which are further transformed into ceramics when heat-treated at higher temperatures.

3.1 Characterization of the powder sample

3.1.1 FT-IR spectral analysis

Figure 1 shows the FT-IR spectra of the as prepared powder and the sample sintered at 900 °C. The FT-IR Spectra for the as dried powder is entirely different from the sintered sample. The as dried powder sample revealed a weak shoulder at 450 cm^{-1}, strong bands at 542 cm^{-1}, and 2,300 cm^{-1}, corresponds to P–O(H) stretching in HPO_4^{2-} groups. Also, the spectrum shows a strong γ_1 and a broad γ_3 mode of P–O vibrations at 1,008 and 1,094 cm^{-1} respectively. The IR spectra for the sample sintered at 900 °C revealed a band at 730 and 1,218 cm^{-1} indicating the presence symmetric and asymmetric stretching of the P–O–P vibrations in $P_2O_7^{4-}$ ions [13–17]. So, this spectrum confirms the dehydration of HPO_4^{2-} into $P_2O_7^{4-}$ ions according to the following reaction.

$$2HPO_4^{2-} \rightarrow P_2O_7^{4-} + H_2O$$

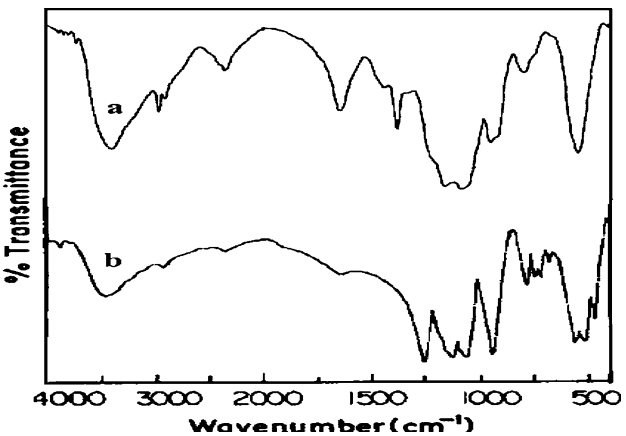

Fig. 1 FT-IR spectra for the powder (**a**) as dried (**b**) sintered at 900 °C

The band around 1,000–1,300 cm^{-1} appears as a quartet with well-resolved peaks at 1,218, 1,096, 1,085, and 1,056 cm^{-1} identical to phosphate bands. The desorption of ethanol with increasing temperature was confirmed by the disappearance of band at 2,830 cm^{-1} which was seen in the as dried powder.

3.1.2 XRD spectrum

Figure 2 denotes the XRD Spectra for the as dried and the sample sintered at 900 °C. The XRD spectrum recorded for the as prepared powder at 150 °C was identical with $CaHPO_4$. The as dried powder was completely amorphous and the appearance of a single peak at 26.586 with the corresponding h k l value of (2 2 0) indicated the presence of $CaHPO_4$. The powder sintered at 900 °C revealed a strong peak at 29.554 with the corresponding h k l value of (0 0 8) indicates the formation of β-$Ca_2P_2O_7$. All the other pyro phosphate peaks at 28.870 (0 2 3) and 27.681 (0 2 2) was also seen in the XRD spectrum. According to the previous study [18], the $CaHPO_4$ was transformed to β-$Ca_2P_2O_7$ when heat treated at 750 °C. For the sample sintered at 900 °C, the intensity of β-$Ca_2P_2O_7$ peak is very sharp which confirmed the higher crystallinity and the complete conversion of HPO_4^{2-} to $P_2O_7^{4-}$ ions in the sintered sample. Identification of crystalline phases was done by comparing with JCPDS files ($CaHPO_4$: 09-0080 and β-$Ca_2P_2O_7$: 33-0297).

3.2 Characterization of the coating

3.2.1 SEM analysis

The surface morphology of the triple layer coated sample sintered at 800 °C was shown in Fig. 3. SEM morphology of the triple layer coating showed a uniform distribution of particles over metallic substrate, which indicates that the coatings are very dense in nature. The thickness of the triple layer coating sintered at 800 °C was found to be

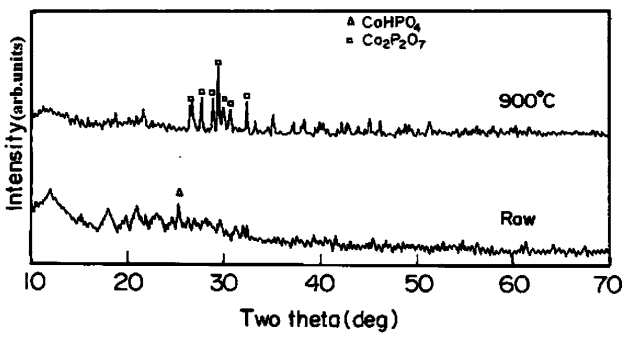

Fig. 2 XRD pattern for the as prepared and the powder sintered at 900 °C

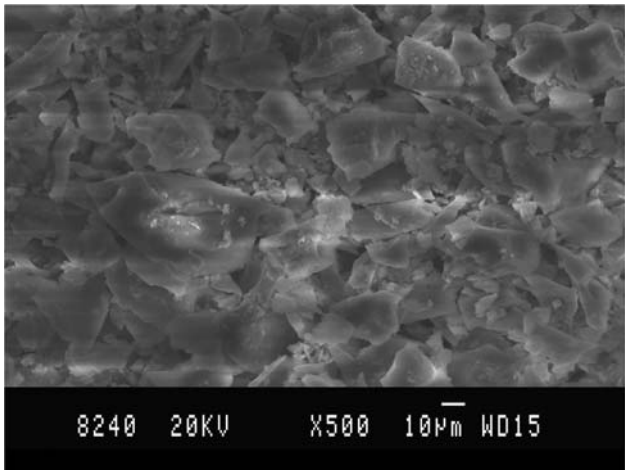

Fig. 3 SEM images for the triple layer coated 316L SS sintered at 800 °C

1 µm and it does not undergo cracking at the optimum spin speed of 2,000 RPM/Min. This behavior suggests that there was less shrinkage in the coating at the optimum spin speed. Whereas the coating sintered at 900 °C undergo cracking due to particle decohesion and thermal mismatch between the coating and the substrate. Several workers have also reported the cracking of sol gel coatings [19–24]. Hence, an optimum thickness of coating is to be arrived at 1 µm.

3.2.2 Adhesion strength of the coating

Adhesion test was performed on the multilayer coatings to yield measurements of coating adherence. The adhesion strength of the coating can provide a useful comparison with the mechanical properties of the surrounding coating and underlying implant. The adhesion strength for the single and triple layer coating sintered at 800 °C was found to be 30 and 46 Mpa, respectively. From Fig. 4, it was confirmed that the triple layer coating sintered at 800 °C was found to be compact and adherent on the metallic surface and this behavior accounts for the corrosion resistance of the coating. The adhesive strength of the epoxy glue (without coating) was about 54 MPa, a value slightly higher than the multilayered coatings. However, due to thermal mismatch between the triple layer coating and the substrate, a decrease in adhesive strength of 39 MPa was obtained for the coating sintered at 900 °C.

3.2.3 EDAX analysis

The surface changes occurred due to glass-ceramic coating was characterized using EDAX analysis. The dynamic proportions of the coating provide a key to the high

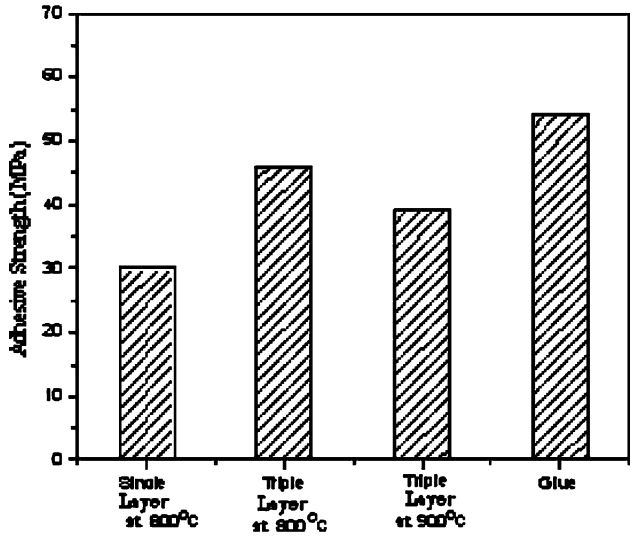

Fig. 4 Adhesive strength for the multilayer coating sintered at different temperatures

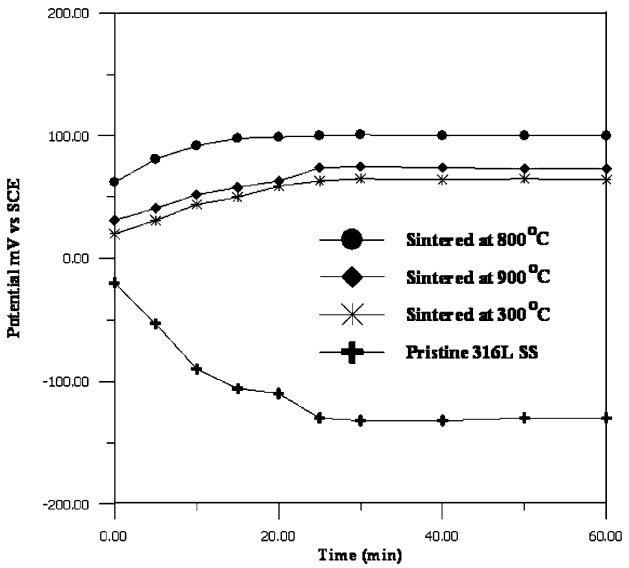

Fig. 6 OCP time measurements for the sol–gel triple layer coating sintered at different temperatures

resistance of 316L SS to corrosive attack. Figure 5 denotes the EDAX spectrum for the triple layer coating sintered at 800 °C. The calcium and phosphorous ratio was found to be 1.00, which could be due to the formation of pyrophosphate ions. The absence of substrate peaks such as Fe, Cr, and Ni represent the stability of the coating sintered at 800 °C.

3.2.4 *Electrochemical evaluation of coating*

OCP measurements: The OCP-time plots for the sol–gel coated 316L SS with various sintering temperatures are shown in Fig. 6. For the uncoated sample, a continuous decrease in OCP towards the active potential of –132 mV was observed. The ceramic coatings obtained at various sintering temperature showed the potential variations in the nobler direction.

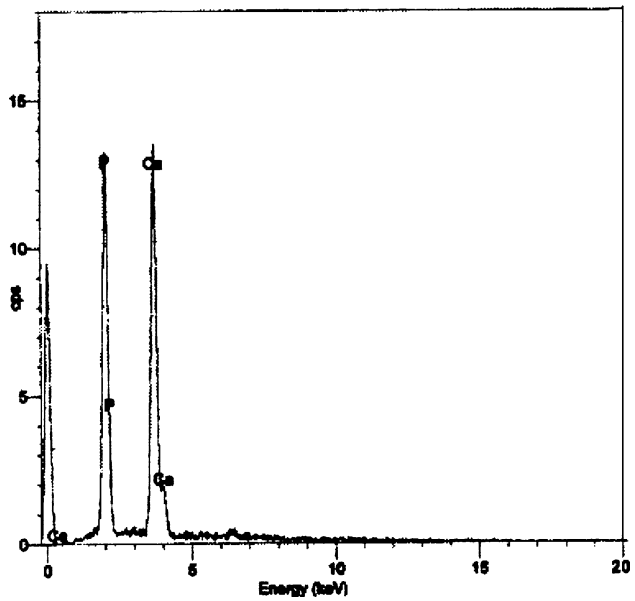

Fig. 5 EDAX Spectrum for the triple layer coating sintered at 800 °C

Cyclic polarization study: The cyclic polarization curves for the multi layer glass-ceramic coating sintered at different temperatures are shown in Fig. 7. Sol–gel coated 316L SS indicated a remarkable shift in the nobler direction when compared with pristine 316L SS. The electrochemical parameters E_b and E_p obtained from cyclic polarization study are presented in Table 3.

From Table 3, it is clear that all the coated substrates recorded a maximum E_b and E_p value than pristine 316L SS. The uncoated 316L SS showed lower corrosion resistance with the E_b value of +320 and E_p value of –80 mV and higher current density (32 μA/cm^2) in the physiological solution. The breakdown potential for the triple layer coated sample sintered at 800 °C showed a maximum value of +826 mV and the repassivation potential of +222 mV respectively. The current density for this coating was found to decrease from 32 μA/cm^2 (for pristine 316L SS) to 3.8 μA/cm^2. The reason for the shift is due to the presence of adherent coating layer with the strength of 46 MPa between the ceramic and the metal, which resists the onset of pitting, when compared to pristine 316L SS. The single layer coating sintered at 800 °C had a significant effect on the corrosion resistance behavior on 316L SS with the current density of 6.4 μA/cm^2. The triple layer coating sintered at 800 °C has shown lower current density than the single layer and the E_b (+826 mV) and E_p (+222 mV) value was found to be high than the single layer

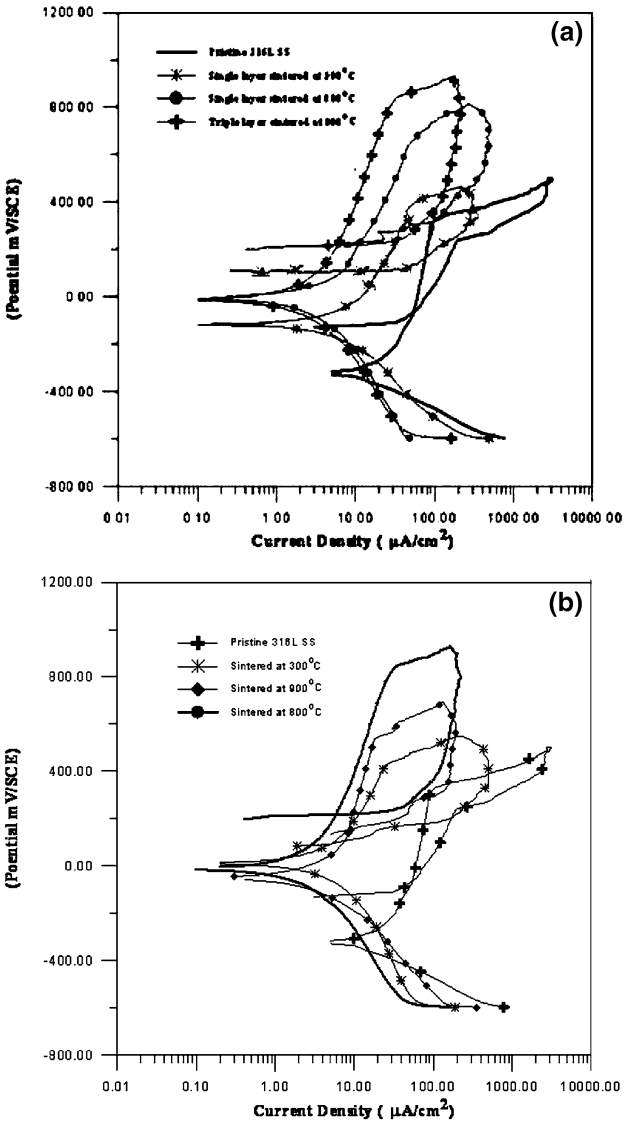

Fig. 7 Cyclic polarization curves for the sol–gel coating on 316L SS. (**a**) multilayer coating (**b**) triple layer coating sintered at different temperatures

coating (E_b = +621 mV, E_p = +218 mV). Even though, the E_p value for the single layer coating was found to be similar than triple layer coating, the lower current density with higher breakdown potential indicates its corrosion resistance behavior.

The multi layer coating has a positive effect on corrosion resistance of metallic substrate. The corrosion resistance behavior of the triple layer coating sintered at 300 °C was higher than the single layer coating, as manifested by the shift in the E_b value of +428 mV with the corresponding decrease in the E_b value for +398 mV for the single layer coating. Therefore, the triple layer coating on 316L SS caused better corrosion resistant behavior in Ringer's solution.

Table 3 Cyclic polarization parameters for the multi layer sol–gel coatings

S. no.	Temperature	Electrochemical parameters		Current density ($\mu A/cm^2$)
		E_b (mV)	E_p (mV)	
1	Pristine 316L SS	+320	–80	32
2	Single layer sintered at 300 °C	+398	+112	9.8
3	Single layer sintered at 800 °C	+621	+218	6.4
4	Triple layer sintered at 300 °C	+428	+90	5.0
5	Triple layer sintered at 800 °C	+826	+222	3.8
6	Triple layer sintered at 900 °C	+532	+108	5.2

After the electrochemical polarization tests, the coated samples were closely analyzed by optical microscope. The delamination of the triple layer coating sintered at 900 °C could be clearly seen along the edge, indicating preferential localized attack and this fact was confirmed by the reduction in the E_b (532 mV) and E_p (+108 mV) values as compared to the coating sintered at 800 °C.

Impedance studies: Electrochemical impedance experiments were performed at the open circuit potential and the spectra obtained for the triple layer coated substrates sintered at different temperatures are shown in Fig. 8. Nyquist and impedance spectra are more informative for the investigation of changes in the electrochemical characteristics of the coated system. From Fig. 8, it was observed that variations in the impedance spectra occurred for the coated substrates, which resulted from the evolution of the electrochemical behavior of the system.

Table 4 shows the electrochemical parameters such as R_{ct} and C_{dl} obtained from impedance study. From the Table, the R_{ct} value (3.200×10^5 ohms) for the coating sintered at 800 °C was found to be higher. A high R_{ct} value is an indication of excellent corrosion resistance due to the deposition of dense coating and this coating can act as a protective coating which is able to strongly reduce both the corrosion attack of the steel and the diffusion of iron release from the substrate. The above fact is also confirmed by the lower value of C_{dl} from 3.380 $x10^{-6}$ F cm^2 for the pristine 316L SS to 0.8818×10^{-6} F cm^2 for the coating sintered at 800 °C substantiates the presence of relatively coherent and stable coating on the surface. A further increase in C_{dl} value (0.9268×10^{-6} F cm^2) for the coating sintered at 900 °C reflects the same results observed by cyclic polarization.

The equivalent circuit used in this model is a series combination of a resistance and a capacitance (the double

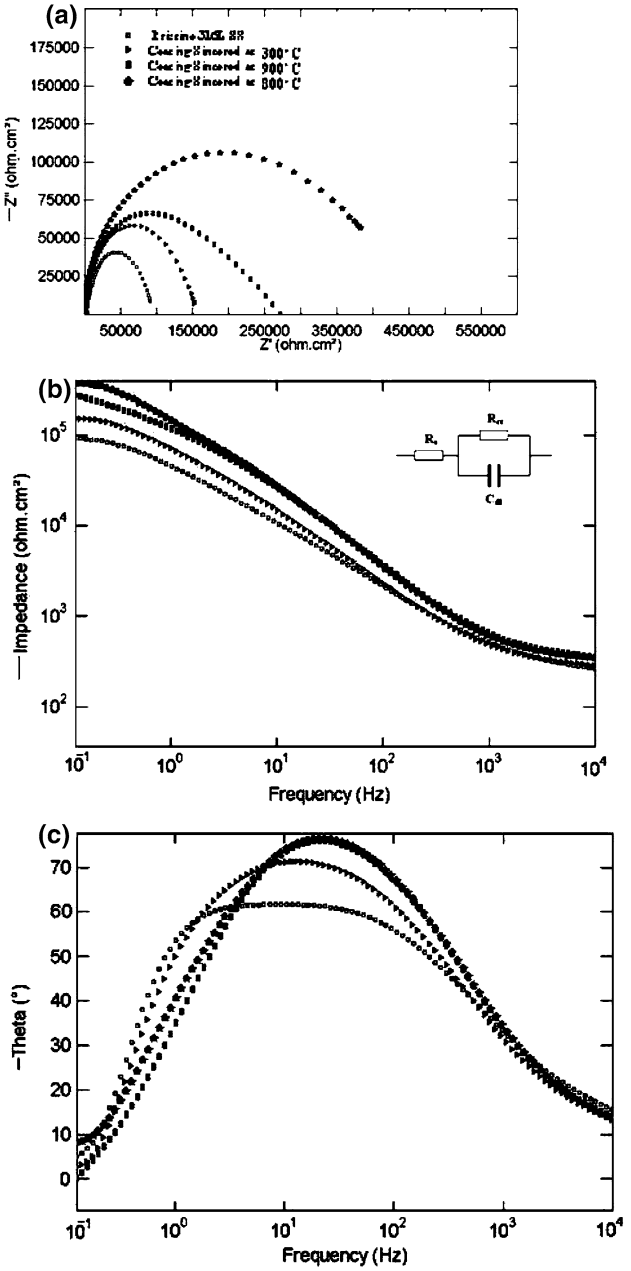

Fig. 8 Nyquist (**a**) and Bode (**b** and **c**) plots of glass-ceramic triple layer coatings sintered at different temperature in Ringers solution at open circuit potential

layer capacitance) and it consists of the following elements: a solution resistance (R_s) of the test electrolyte, the coating capacitance (C_{dl}) of the uniform coating layer, the charge transfer resistance (R_{ct}) which controls the rate of electrochemical processes at the metal/electrolyte interface. Over the frequency range applied the equivalent circuit employed for the description of the coated samples provides the best fitting of the experimental data.

From the Bode spectra, it is possible to predict the stability of the coating from the phase angle. Bode spectra for the uncoated sample exhibited a phase angle of –60°, while the coatings sintered at different temperatures have shown an increase in the phase angle to –75° over a wide frequency range. The shift in phase angle and higher value of R_{ct} value with the corresponding decrease in the C_{dl} value manifests the presence of a more compact and uniform coating formed on 316L SS during heat treatments. The results observed from the two electrochemical techniques were concordant with each other. As the sintering temperature increases, the compactness of the coating was found to be high. The positive shift in the E_b and E_p values with the corresponding decrease in the current density value for the triple layer coating sintered at 800 °C illustrates the presence of more adherent film.

In view of the above fact, that the coatings deposited by the spin coating could be applied for fixation purposes in order to improve the implant-tissue interaction and also to increase the life time of the implantation devices.

Table 4 Electrochemical Impedance parameters for the triple layer coating sintered at different temperatures

S.no	Temperature	Electrochemical parameters	
		Charge transfer resistance $R_{ct} \times 10^5$ (ohms)	Double layer capacitance $(C_{dl}) \times 10^{-6}$ (F cm^2)
1	Pristine 316L SS	0.9819	3.380
2	Triple layer Sintered at 300 °C	0.9834	3.239
3	Triple layer Sintered at 800 °C	3.200	0.8818
4	Triple layer Sintered at 900 °C	1.792	0.9268

4 Conclusion

From the results presented above, it can be concluded that the uniform and adherent coating was deposited on 316L SS by spin coating method at the optimum spin speed of 2000 RPM/Min. The triple layer coated 316L SS showed uniform surface morphology with the coating thickness of 1 μm. The adhesion strength for the triple layer coating sintered at 800 °C was found to be 46 MPa.

Electrochemical characterization of the triple layer coated 316L SS showed a dramatic reduction in the current densities and an increase in E_b and E_p value towards nobler direction compared with the uncoated alloy. The result obtained from EIS study, have demonstrated the stability of the coatings by the increase in the R_{ct} value from 0.9816×10^5 to 3.200×10^5 ohms. The combined effect of adherence with higher corrosion resistance of the glass coating acts as a diffusion barrier and can be used as a potential material for implantation purposes.

References

1. Hench LL (1991) J Am Ceram Soc 74:1485
2. Niinomi M, Kuroda D, Fukunaga K, Morinaga M, Kato Y, Yashiro T, Suzuki A (1999) Mater Sci Technol A 263:193
3. Guglielmi M (1994) J Sol-gel Sci Tech 1:177
4. Simoes M, Assis OBG, Avaca LA (2000) Ibid 273:159
5. Atik M, Messaddeq SH, Luna FP, Aegerter MA (1996) J Mater Sci Lett 15:2051
6. Vasconcelos DCL, Carvalho JN, Mantal M, Vasconcelos WL (2000) J Non-Cryst Solids 273:135
7. Craig RG, Powers JM, Wataha JC (2000) Dental materials, properties and manipulation, 7th edn. Mosby-Year book Inc., St. Louis, p 231
8. El-Ghannam A, Ducheyne P, Shapiro M (1997) J Biomed Mater Res 36:167
9. Garcia C, Cere S, Duran A (2004) J Non-Cryst Solids 348:218
10. Chin TS, Wu DC, Hang MP, Wang CP (1996) J Mater Res 11:962
11. Weng W, Baptista JL (1997) J Sol-gel Sci Technol 8:645
12. Livage J, Barboux P, Vandenborre MT, Schmutz C, Taulell F (1992) J Non-Cryst Solids 147–148:18
13. Nakamoto K (1963) Infra red spectra of inorganic and coordination compounds. John Wiley and Sons, Newyork, p 197
14. Cornilsen BC, Condrate RA (1978) J Inorg Nucl Chem 41:602
15. Layrolle P, Lebugle A (1994) Chem Mater 6:1996
16. Metwalli E, Brow RK (2001) J Non-Cryst Solids 289:113
17. Exarhos GJ, Miller PJ, Risen WM (1974) J Chem Phy 60:4145
18. Manso M, Martinez-Duart JM, Langlet M, Jimenez C, Herrero P, Millon E (2002) J Mater Res 17:1482
19. Jordan JD, Dunbar RA, Hook DJ, Zhuang H, Gardella JA, Colo LA Jr, Bright FV (1998) Chem Mater 10:1041
20. Chen W, Zhang J, Fang Q, Li S, Wu J, Li F, Jiang K (2004) Sens Actuators B 100:195
21. Huang Y-Y, Chou K-S (2003) Ceramics Int 29:485
22. Chan CM, Cao GZ, Fong H, Sarikaya M (2000) J Mater Res 15:148
23. Jeong S, Janga W-H, Moon J (2004) Thin Solid Films 466:204
24. Gomez-Vega JM, Iyoshi M, Kim KY, Hozumi A, Sugimura H, Takai O (2001) Thin Solid Films 398–399:615